Sensors & Actuators: B. Chemical 321 (2020) 128454

Contents lists available at ScienceDirect

Sensors and Actuators B: Chemical

journal homepage: www.elsevier.com/locate/snb

Electrochemiluminescence sensing platform based on functionalized poly-(styrene-co-maleicanhydride) nanocrystals and iron doped hydroxyapatite for CYFRA 21-1 immunoassay

Jingwei Xue[a], Lei Yang[a], Yu Du[a], Yong Ren[b], Xiang Ren[a], Hongmin Ma[a], Dan Wu[a], Huangxian Ju[a], Yueyuan Li[a,*], Qin Wei[a,*]

[a] Collaborative Innovation Center for Green Chemical Manufacturing and Accurate Detection, Key Laboratory of Interfacial Reaction & Sensing Analysis in Universities of Shandong, School of Chemistry and Chemical Engineering, University of Jinan, Jinan 250022, China
[b] Department of Mathematical Sciences, Zibo Normal College, Zibo Shandong 255130, China

ARTICLE INFO

Keywords:
Electrochemiluminescence
Aggregation induced emission
Quenching platform
Tetraphenylethylene
Iron doped hydroxyapatite

ABSTRACT

This report outlines a versatile novel quenching electrochemiluminescence immunosensor based on electrochemiluminescence (ECL) emission with aggregation induced emission (AIE) from TP－COOH NCs, which was utilized by poly-(styrene-co-maleicanhydride) to wrap on tetraphenylethylene nanocrystals. On the one hand, the cathode emission excited at -1.15 V could reduce emission produced by oxygen from high potential stimulation, on the other hand, such low potential can further protect the activity of immune molecules. Meanwhile, the coating can reduce interface impedance and completed functionalization. Herein, based on the synergistic effect of electron transfer and energy transfer between TP－COOH NCs and iron doped hydroxyapatite (Fe-HAP), the high efficiency of this ECL sensing platform can be achieved. The proposed ECL immunosensor for detection of trace Cytokeratin 19 fragment 21－1 (CYFRA21－1), exhibited a satisfied detection limit low to 0.01471 pg/mL ($S/N = 3$). As a result, this approach not only enriches the ECL strategies study to provide a feasible method for foundational clinical examination but also expands the potential application of ECL sensors in biological testing and clinical high-throughput diagnosis.

1. Introduction

Lung cancer is the highest incidence and death rate of malignant tumors in the world, and its incidence and death rate are rising all the time. Non-small cell lung cancer (NSCLC) accounts for more than 80 % of all lung cancer cases [1]. The mortality of lung cancer is about 88 % according to the world health organization [2]. Compared with small cell carcinoma, the cancer cells grow and divide more slowly and spread and metastasize later [3]. Therefore, it is super crucial to timely and accurate diagnosis of NSCLC patients. In clinical analysis, the detection of tumor markers, Cytokeratin 19 fragment 21－1 (CYFRA21－1), whose level is related to the type and severity of tumor, has caused great concern [4].

Up to now, electrochemiluminescence (ECL) biosensors have been developed for the detection of biomarkers due to its high detection sensitivity, low optical devices cost and wide linear range [5–8]. Various nanomaterials were applied as carriers to make traditional ECL luminophores immobilization and more and more novel ECL emitter were obvious and prepared [9,10], such as semiconductor quantum dots (QDs) (CdSeTe, CdTe, PbS, etc) and metallic nanoclusters (NCs) [11]. But their distinct disadvantages of poor biocompatibility or high cost limit their application and development [12,13]. Therefore, the new improved organic nanoparticles (NPs) have received more and more attention [14].

It is known that a series of ECL nanomaterials were synthesized with precursors, polycyclic aromatic hydrocarbons (PAHs) [15,16], which could accumulate plentifully in dense ECL nanomaterials to enhance the ECL signal [17,18]. According to recent research [19], aggregation induced ECL enhanced emission (AIE) which inspired by propeller-like fluorophils has been attracted attention [20]. From Yuan's group [21], the ECL emitter, tetraphenylethylene nanocrystals (TPE NCs) demonstrated excellent response with existence of triethylamine (TEA). Nevertheless, there are two notable aspects: 1. Bovine serum albumin was wrapped on the TPE NCs to offer a hydrophilic surface but the resistance of proteins to electron transfer should be noticed. 2. The TPE/TEA system can be excited at the potential of +1.5 V which is so

* Corresponding authors.
E-mail addresses: yueyuanli86@163.com (Y. Li), sdjndxwq@163.com (Q. Wei).

https://doi.org/10.1016/j.snb.2020.128454
Received 3 April 2020; Received in revised form 6 June 2020; Accepted 10 June 2020
Available online 20 June 2020
0925-4005/

high that cause irreversible damage to immune factors [22]. In order to solve these problems, TPE NCs were firstly prepared by using poly-(styrene-co-maleicanhydride) (PSMA) which can also wrap the carboxyl group on (TP − COOH NCs) and a strong signal was obtained at the potential of -1.15 V in the system of TP − COOH NCs/$K_2S_4O_8$. This method can not only improve the barrier of protein to the electron transmission process, but also avoid the damage caused by over-potential to the immune content. The anode ECL excitation at 0 ~ + 1.15 V was also tested and compared, and it is shown that the cathode excitation effect was superior to consider biological activity.

Moreover, hydroxyapatite (HAP), a potential material with good biocompatibility, has been widely used in biomedical, biotechnological and environmental fields [23]. Due to its special crystal chemical characteristics, a variety of metallic cations can remain in HAP. The generated metal-doped HAP not only retains the original biocompatibility [24], but also plays the role of ions. Among them, Fe^{3+} doped HAP (Fe-HAP) is a blood compatible biomaterial [25]. Its superior performance can directly mark biological signal molecules [26].

Fortunately, the ECL spectra of TP − COOH and the UV–vis absorption spectrum of Fe-HAP possess effective area overlap. Furthermore, TP − COOH NCs has a wide band gap and the REDOX potential of Fe^{3+}/Fe^{2+} is in this band gap, which allows electron transfer between Fe^{3+} and TP − COOH NCs anion radical, thus causing quenching effect [27]. It is worth mentioning that biocompatible TP − COOH NCs were put forward in ECL field at a low excited potential of -1.15 V for the first time and quenched by energy transfer and electron transfer, based on protecting the activity of immune molecules, and increasing the efficiency of electron transmission [28]. Furthermore, protein A was used for improving incubation efficiency, thus enhanced biosensor sensitivity. Herein, we used CYFRA21 − 1 as a detection target to analysis of the test, which could provide a reference for the analysis method.

2. Experimental section

2.1. Preparation of TP − COOH nanocrystals (NCs)

Briefly, TPE powder (4.0 mg) and 4.0 mL of tetrahydrofuran (THF) were mixed to gain the homogeneous colorless TPE solution (1.0 mg/mL). The same concentration of PSMA (2 mg) was prepared. Then 4.0 mL of the prepared TPE solution and 1 mL of PSMA were mixed under sonication to form a homogeneous solution, followed by stirring for 2 h at room temperature. Finally, the TP − COOH NCs were obtained.

2.2. Preparation of Fe-HAP

1.0 g of HAP and 1.8 g $Fe(NO)_3$ were dissolved in 100 mL distilled water. The resulting mixture was stirred continuously at 25 ℃ for 15 min. The suspension was washed by deionized water for three times. The precipitated particles were dried at 100 ℃ for 8 h in air followed by grinding and yellow powder, Fe-HAP was obtained. Fe-HAP-Ab_2 biological complex was further synthesized in Supplementary Material.

2.3. Immunosensor fabrication

Firstly, the bare GCE after pretreatment was anchored with 6 μL of TP − COOH NCs. Next, GCE/TP − COOH NCs was disposed by 0.01 M EDC/NHS (1:1) to make carboxyl groups activated on the surface. The resultant electrode was dripped onto 5 μL of protein A solution (50 μg/mL) to couple antibody capturer via amidatio and soaked in the 4 μg/mL of Ab_1 at 4 ℃. Subsequently, 3 μL of BSA (0.1 %) was cast onto the surface and 6 μL of CYFRA 21 − 1 with concentration gradient was incubated at 37 ℃. After the last incubation step of 6 μL of Fe-HAP-Ab_2, the obtained biosensor was ready for detection [29]. The schematic graph of assembly process was illustrated in Scheme 1.

2.4. ECL measurements and actual sample testing

The ECL responses were investigated with three-electrode system (Supplementary Material) in 10 mL of $K_2S_4O_8$ (1 mM, pH 7.4). The photomultiplier tube (PMT) voltage was at 850 V and the working potential was -1.15 ~ 0 V (vs. Ag/AgCl) with 0.15 V/s scanning rate. The proposed electron transfer strategy between TP − COOH and Fe-HAP was utilized to measure different concentrations CYFRA21 − 1 from 1×10^{-7} to 500 ng/mL. For actual sample testing, the human serum sample was diluted by pH 7.4 PBS buffer solution to the calibration range. After determining the PCT concentration in the diluted serum sample, PCT standard solutions were added into the diluted samples.

3. Results and discussion

3.1. Characterization of materials

The polystyrene nanoparticles were shown an average size of 200 nm by scanning electron microscope (SEM) (Fig. 1A), which further proofed by using transmission electron microscopy inset of Fig. 1A. When PSMA was coated onto polystyrene nanoparticles, transmission electron microscopy (TEM) images (Fig. 1B) could present average diameter of 250 nm and the lattice shown by high-resolution transmission electron microscopy (HRTEM) is no longer visible clearly inset of Fig. 1B, although there is no significant change in morphology. X-Ray diffraction (XRD) (Fig. 1C) played a role in characterizing crystallization of TPE and TP − COOH NCs. The PSMA coating did not cause damage to the crystalline structure of the TPE. The same tests were done for Fe-HAP which proved successful ion-exchange between Fe^{3+} and Ca^{2+}. Compared with pure HAP, Fe^{3+} was uniformly embedded in the apatite and without any impacts on other elements. As shown in Fig. 1F, XRD could present no effect of the HAP lattice when doping of Fe^{3+}. TEM (Fig. 1D) and HRTEM (Fig. 1E) were also utilized on Fe-HAP, which could observe the nanocrystalline structure and clear lattice. EDX mapping (Fig. 1G) was applied on Fe-HAP, which could present of Fe, Ca, O, and P elements clearly.

To further demonstrate the successful doping of Fe and analyze the chemical composition and element state, X-ray photoelectron spectroscopy (XPS) of Fe-HAP was supplied. The major XPS peaks of Fe-2p, Ca-2p and P-2p levels were clearly observed in Fig. 2A. About the spectrum of Fe 2p (Fig. 2B), both peaks, which gave the credit to Fe $2p_{1/2}$ and Fe $2p_{3/2}$ of Fe^{3+}, were well presented at 725.7 eV and 712.5 eV, with two satellite peaks detecting at 734.2 eV and 718.5 eV [30]. As well, the two others at 723.5 eV and 716.0 eV were attributed to Fe^{2+}, with their satellite peaks displaying at 729.3 eV and 716.0 eV [31]. Two peaks were with respect to Ca $2p_{1/2}$ and Ca $2p_{3/2}$ of Ca^{2+} (Fig. 2C) in HAP which situated at 351.4 eV and 347.5 eV and the spectra of P 2p (Fig. 2D), and one peak was identified at 134.1 eV in Fe-HAP, which should be owing to the phosphate [32].

3.2. Characterization of ECL immunosensor

The diff ;erent fabricated electrodes of the biosensor were demonstrated a multi-modal assay in 2.5 mM $[Fe(CN)_6]^{3-/4-}$ including 0.1 M KCl. by using cyclic voltammetry (CV) and electrochemical impedance spectroscopy (EIS) (Fig. 3A). Firstly, curve a was produced small impedance value owe to diff ;usion of bare GCE. Successively, modified TP − COOH, dripped into protein A, Ab_1 and cast on BSA, CYFRA 21 − 1, and finally Fe-HAP − Ab_2 (curve b to curve g). The impedance value maintained a continuous increase, especially after attaching immune molecules because the protein reduced the efficiency of electron transfer on the surface of the electrode [33]. Moreover, simulation parameters equivalent circuit element shown in Table S1 was simulated. CV scanning (Fig. S2) also further reflected the current changes on different electrode surfaces, and these two analysis methods supported each other to prove the successful construction of the sensor.

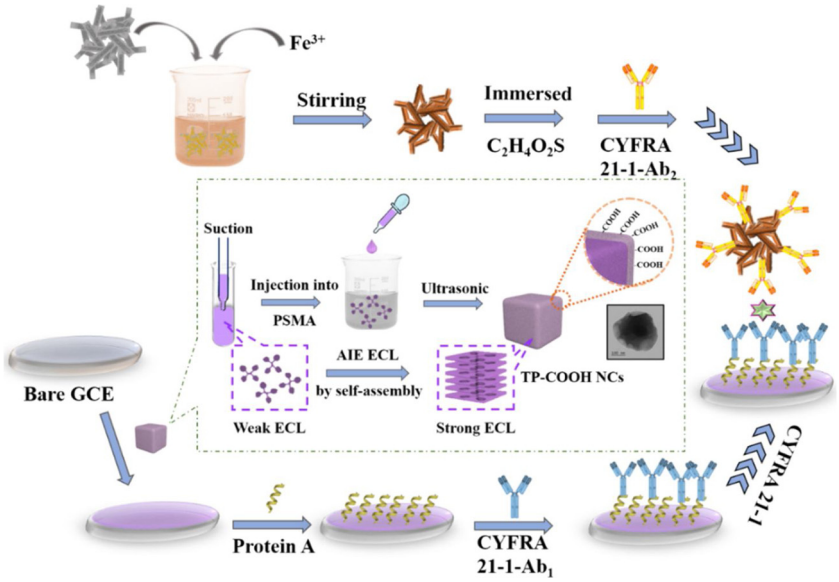

Scheme 1. Mechanism of fabrication of immunosensor and introduction.

Moreover, it could be seen that the TP – COOH coating with PMSA (red curve) owned a negatively shifted anodic potential (0.362 V) and a greatly increased anodic current, which means that using PMSA as protection and functional reagent is more beneficial to the electron transfer on the electrode surface than using BSA (Fig. 3B) and the collected circular dichroism (CD) data (Fig. 3C) displayed the comparison of protein activity after different potential stimulation.

3.3. Mechanism investigation of the "signal-off" system

TP – COOH turned out to be a well ECL response when $K_2S_2O_8$ existed. According to previous reports on the mechanism of cathode ECL excited [34], the possible ECL mechanisms analogous to the pathways of other semiconductors were speculated with the following equations:

$$TP-COOH + e^- \rightarrow TP-COOH^{\cdot}\text{-}$$

$$S_2O_8^{2-} + e^- \rightarrow SO_4^{\cdot -}$$

$$SO_4^{\cdot -} + TP-COOH^{\cdot -} \rightarrow TP-COOH\ ^* + SO_4^{2-}$$

and/or

$$TP-COOH + SO_4^{\cdot -} \rightarrow TP-COOH^+ + SO_4^{2-}$$

$$TP-COOH^+ + TP-COOH^{\cdot -} \rightarrow TP-COOH\ ^* + TP-COOH$$

finally,

$$TP-COOH\ ^* \rightarrow TP-COOH + hv$$

Herein, an electron was injected to the conduction band of TP – COOH from the working electrode on the electrically excited state, then the negatively charged semiconductor TP – COOH was produced (i.e., $TP-COOH^{\cdot -}$). During the cathode scan, electrons may be injected into the conduction band of TP – COOH when the potential is negative. In this way, if the potential at the working electrode is negative when compared with that of the conduction band of TP – COOH, electrons at the carbon paste electrode may transfer to the conduction band of TP – COOH. It makes oxidation of TP – COOH to $TP-COOH^{\cdot -}$ and $S_2O_8^{2-}$ to $SO_4^{\cdot -}$ possible. The excited state TP – COOH * was generated by electron transfer between $TP-COOH^{\cdot -}$ and $SO_4^{\cdot -}$ and when it returns to the ground state, ECL response was obtained. What's more, the responses of cathode and anode excitation in different potential ranges were also tested, which suggested cathode emission at low potential more beneficial (Fig. 5A).

When it is mentioned on the "signal-off" step, ECL intensity of the GCE/TP – COOH-Ab_1/BSA/CYFRA21 – 1 modified carbon paste electrode was eff ;ectively quenched by different concentrations of Fe-HAP in 10 mL of 1 M $K_2S_2O_8$ (pH 7.4). Based on this, two possible quenching mechanisms were speculated: 1. The RET between TP – COOH and Fe-HAP occurred owing to their matching energy levels. 2. The redox potential of Fe^{3+}/ Fe^{2+} may be lying between the conduction and valence bands of TP – COOH, which could allow efficient electron transfer from TP – COOH to Fe^{3+}. For the first possibility, compared with the ECL spectra of TP – COOH and the UV–vis absorption spectrum of Fe-HAP, the observed effective spectral overlap may not be negligible (Fig. 5B). On the second aspect, Mott-Schittky curve (inset of Fig. 5C) and UV–vis diffuse reflection of TP – COOH were used to search for quenching principles. The conduction band potential was calculated as -0.82 V relying on the fact that the flat band was 0.1 V higher than flat band potential. The value of band gap of TP – COOH (3.06 V) were figured out and its valent band (2.24 V) was inferred at the same time (Fig. 5C). The redox potential of Fe^{3+}/ Fe^{2+} (0.771 V vs NHE) was between the TP – COOH conduction (−0.82 V) and valence bands (2.24 V), which provided the conditions for efficient electron transfer from the negatively charged TP – COOH to Fe^{3+} to receive quenching result. It is worth mentioning that a brief schematic diagram of the principle was presented in Fig. 4. Moreover, Stern-Volmer equation was established to describe the quenching mechanism. As concentration of Fe-HAP promoted, the ECL intensity declined (Fig. 5D). The plot of I_0 (ECL intensity without Fe-HAP)/I (ECL intensity with Fe-HAP) versus concentrations of Fe-HAP with scope of 0.05–5 g/L was shown inset of Fig. 5D. Meanwhile, $6.352 \times 10^5\ g^{-1}$ was the value measured of the quenching constant (K_{sv}).

3.4. CYFRA21 – 1 analysis and analysis of real sample

The raw data and the canonical plotting for different concentrations CYFRA21 – 1 were exhibited respectively in Fig. 6A and B. The standard curve, $I_{ECL} = 5681.08 - 1865.24 \times \lg\ c$ ($R^2 = 0.995$), with detection limit of 0.01471 pg/mL ($S/N = 3$), applied log c as X-axis and ECL intensity I_{ECL} as Y-axis. The low limit detection obtained by this system could provide certain application and detection value to CYFRA21 – 1 and other biomarkers.

The real serum sample analysis could summarize the biosensor potential richly. Herein, the value of CYFRA21 – 1 detected in obtained human serum was 1.35 ng/mL. Standard recovery method was verified

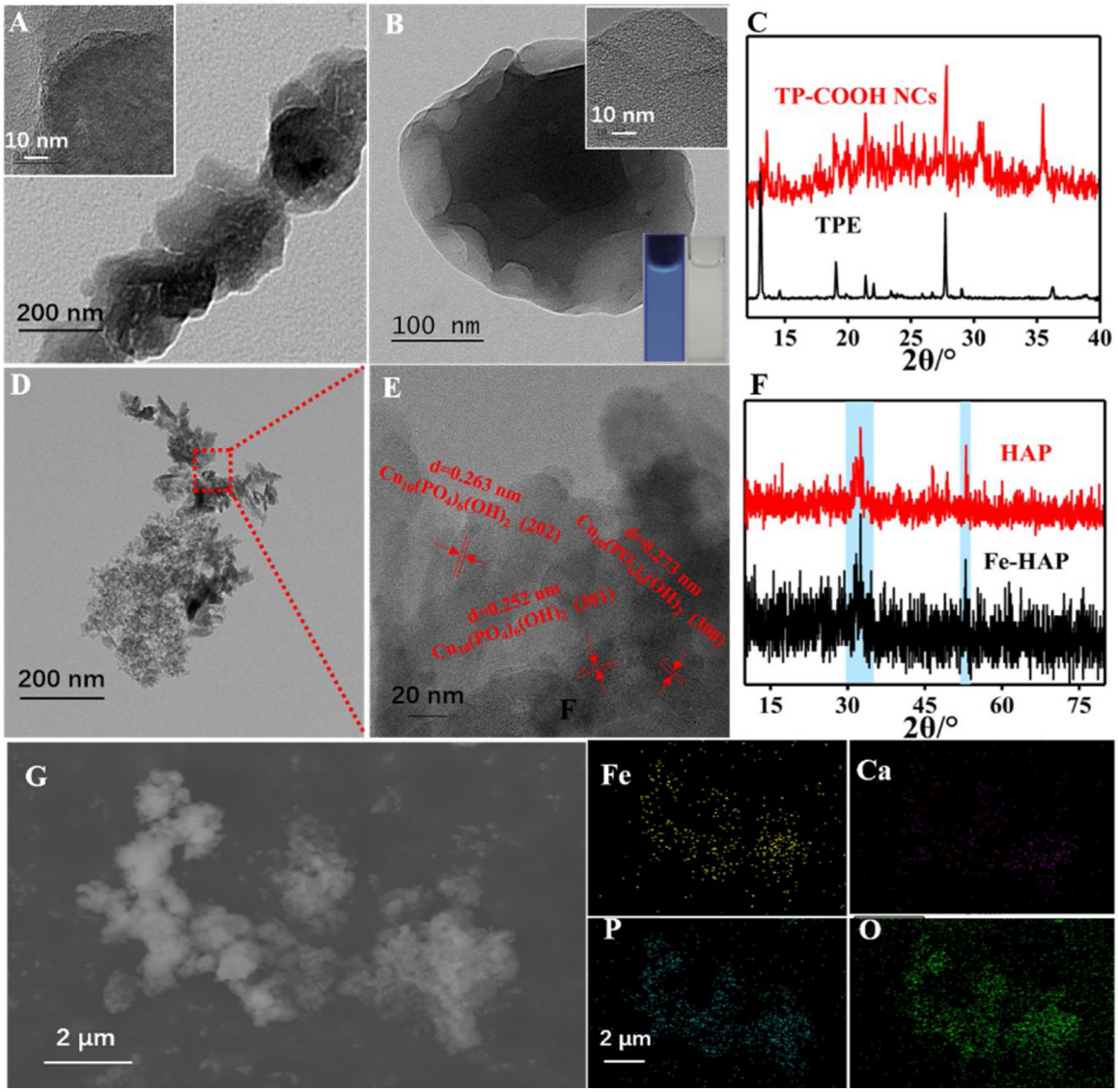

Fig. 1. SEM image of polystyrene nanoparticles and its HRTEM inset of (A), TEM image of TP − COOH NCs and its HRTEM inset of (B), XRD spectra of TPE and TP − COOH NCs (C), TEM (D) and HRTEM (E) spectra of Fe-HAP, XRD spectra of HAP and Fe-HAP(F), SEM mapping of Fe-HAP (G).

by the recovery rate, which displayed range from 99.0%–102.6% (n = 5) with RSD below 3.07 % (Table 1). F-test, which was calculated at 1.27, performed to judge whether consisted in prominent accuracy difference (theoretical value of $F = 6.39$ with 95 % confidence limits). Both methods provided well equivalent precisions, where s represented for the standard deviation. Meanwhile, ELISA kit for five times was also assessed respectively with human serum. There was no significant difference between the mean value of standard recovery and that of ELISA. The t value was calculated at 1.49 (under 2.57, P = 0.95, α = 0.05, f = 4) by using T-test (Table S3), which informed systemic error could be neglect. The precision and accuracy can be guaranteed by utilizing F-test and *t*-test.

$$F = \frac{S_{big}}{S_{little}} \quad (1)$$

$$t = \frac{|\bar{x} - \mu|}{s}\sqrt{n} \quad (2)$$

4. Conclusion

In summary, this paper reports for the cathode ECL emission responses of TP − COOH NCs firstly, and confirmed that it could participate in a novel, valid and promising ECL strategy. Meanwhile, a high-performance ECL platform has been constructed based on electron transfer by good energy level matching and energy transfer by spectral well-overlap between TP − COOH NCs and Fe-HAP. Even more delightful, the proposed system obtained detection limit low to 0.01471 pg/mL ($S/N = 3$). Finally, trace biomarkers, CYFRA21 − 1, have been successfully detected in real serum sample without the serum sample purification and satisfied results were obtained. In general, this obtained ECL assay platform is versatile, facile, ultrasensitive, recyclable, and sufficiently straightforward for trace biomarker detection in complex biological samples, which portended this work can open new avenues to employ ECL systems for sensitive detection of various biomolecules and provide some reference value for related research.

Author's Contribution

All the authors discussed the results and commented on the manuscript.

CRediT authorship contribution statement

Jingwei Xue: Conceptualization, Data curation, Investigation,

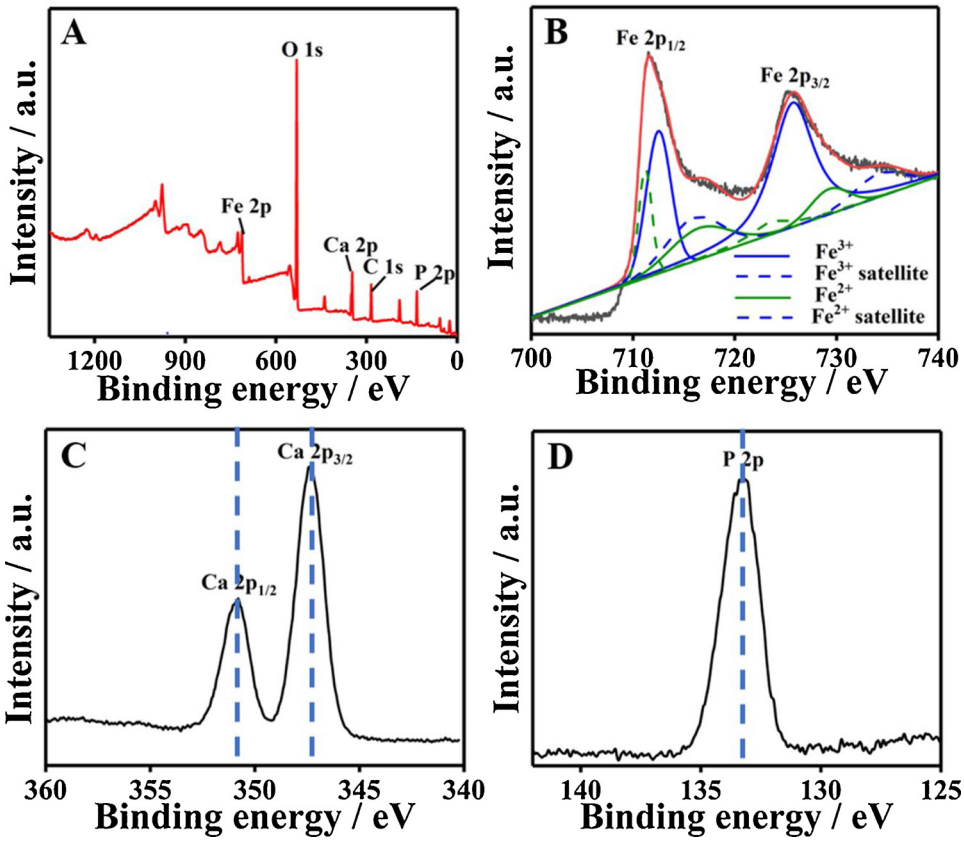

Fig. 2. XPS analyses for full region of Fe-HAP (A), Fe 2p region (B), Ca 2p region (C), P 2p region (D).

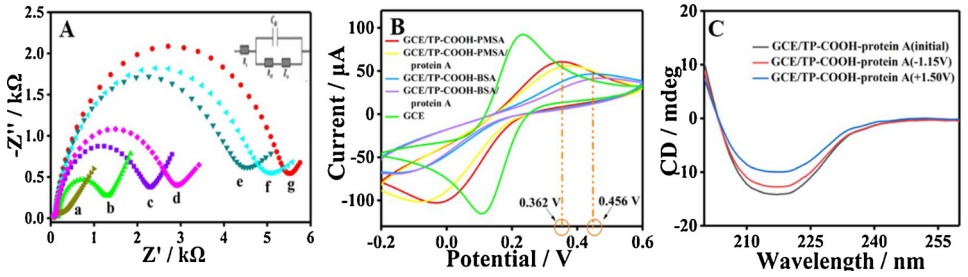

Fig. 3. EIS (A) responses of biosensor with different states of: (a) bare GCE, (b) GCE/TP－COOH, (c) GCE/TP－COOH-protein A, (d) GCE/TP－COOH-protein A/Ab_1, (e) GCE/TP－COOH-protein A/Ab_1/BSA, GCE/TP－COOH-protein A/Ab_1/BSA/CYFRA 21-1, (g) GCE/TP－COOH-protein A/Ab_1/BSA/CYFRA 21-1/Fe-HAP. (B) CV responses of different electrode states. (C) CD contrast of different potential excited.

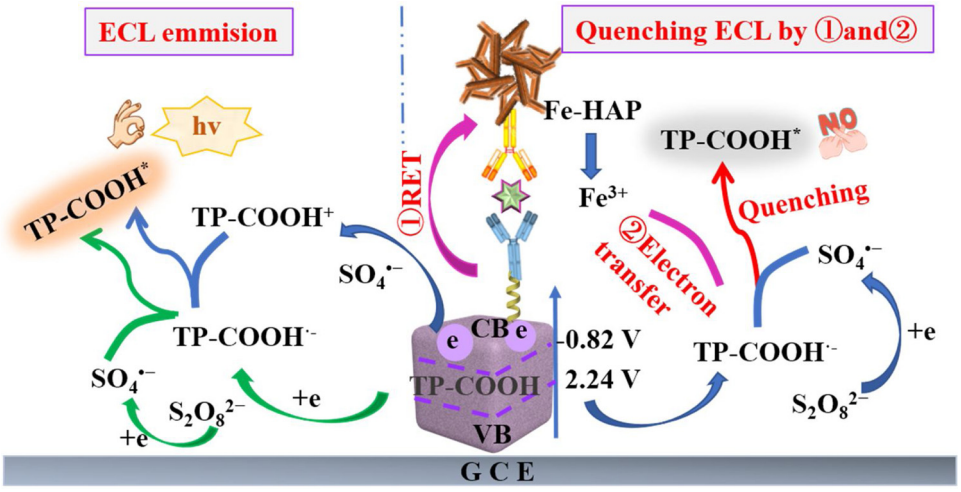

Fig. 4. The reaction pathway of the designed ECL sensor.

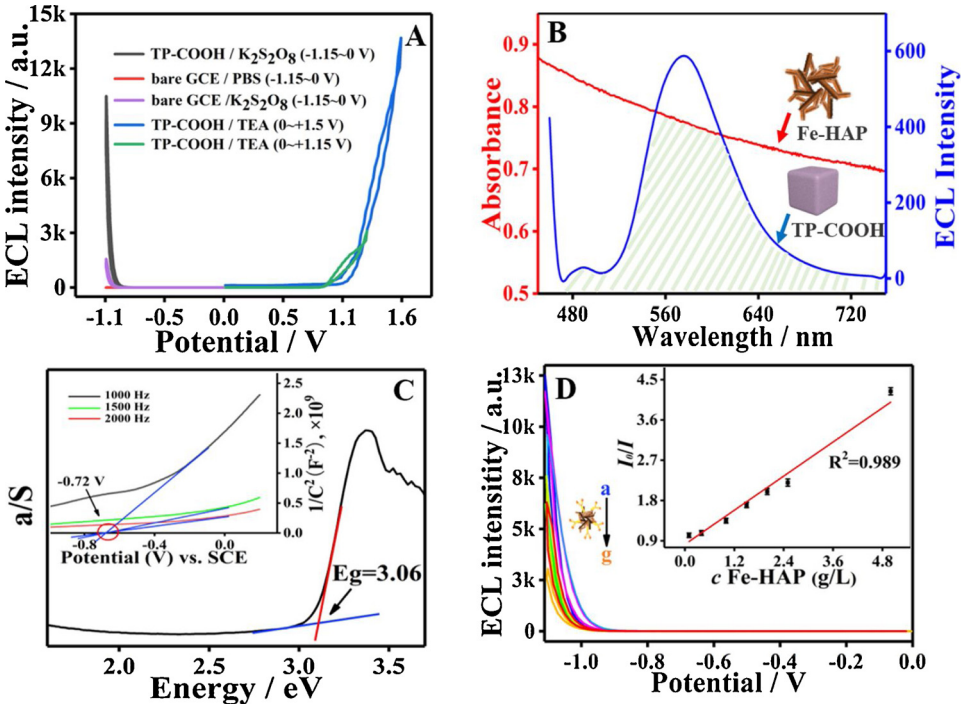

Fig. 5. (A) The responses of cathode and anode excitation in different potential ranges, the overlap curve of TP－COOH ECL spectra and Fe-HAP UV–vis absorption spectrum (B), Mott-Schittky curve (inset of C) and UV–vis DRS (C) of TP－COOH, the ECL intensity with serial concentration of Fe-HAP modification (D) and the graph of I_0/I vs concentrations of Fe-HAP (inset of D).

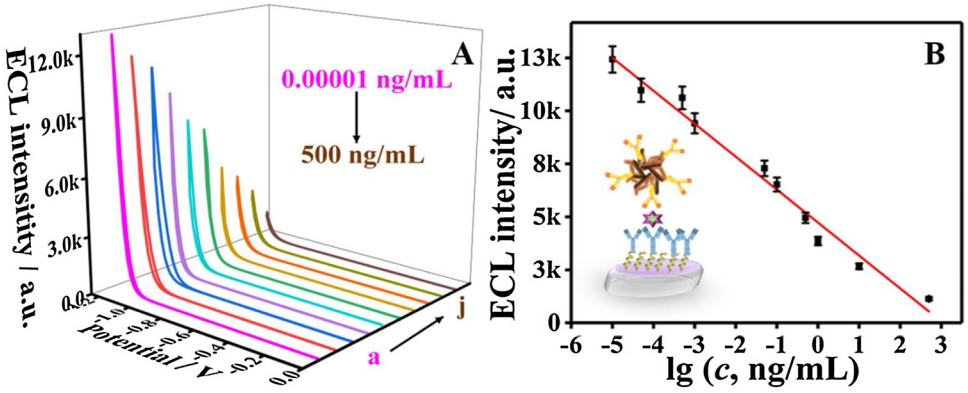

Fig. 6. Detection of CYFRA 21-1 with concentrations from 1×10^{-7} to 500 ng/mL (A) and revealed the canonical plotting (B) which detected in $K_2S_2O_8$ (1 M, pH 7.4).

Table 1
The recovery rate of CYFRA21-1 in serum.

Sample (ng/mL)	Addition content (ng/mL)	Detection content (ng/mL)	RSD (%, n = 5)	Recovery (%)
1.35	1.00	2.46, 2.52, 2.38, 2.13, 2.22	5.69	99.0
	3.00	4.39, 4.41, 4.43, 4.57, 4.35	1.54	102.6
	5.00	6.48, 6.32, 6.25, 6.53, 6.34	1.49	100.6

Visualization, Writing - original draft. **Lei Yang:** Formal analysis, Methodology. **Yu Du:** Formal analysis, Methodology. **Yong Ren:** Conceptualization, Formal analysis, Methodology. **Xiang Ren:** Supervision, Writing - review & editing. **Hongmin Ma:** Supervision, Writing - review & editing. **Dan Wu:** Supervision, Writing - review & editing. **Huangxian Ju:** Supervision, Writing - review & editing. **Yueyuan Li:** Project administration, Resources. **Qin Wei:** Project administration, Resources.

Declaration of Competing Interest

The authors declare that they have no known competing financial interests or personal relationships that could have appeared to influence the work reported in this paper.

Acknowledgements

This study was supported by the National Key Scientific Instrument and Equipment Development Project of China (No. 21627809), National Natural Science Foundation of China (Nos. 21777056), Special Foundation for Taishan Scholar Professorship of Shandong Province, Jinan Scientific Research Leader Workshop Project (Nos. 2018GXRC024, 2018GXRC021) the Innovation Team Project of Colleges and Universities in Jinan (No. 2019GXRC027).

Appendix A. Supplementary data

Supplementary material related to this article can be found, in the online version, at doi:https://doi.org/10.1016/j.snb.2020.128454.

References

[1] P. Goldstraw, D. Ball, J.R. Jett, T.L. Chevalier, E. Lim, A.G. Nicholson, et al., Non-small-cell lung cancer, Lancet 378 (2011) 1727–1740.

[2] K. Dohmoto, S. Hojo, J. Fujita, Y. Yang, Y. Ueda, S. Bandoh, et al., The role of caspase 3 in producing cytokeratin 19 fragment (CYFRA21-1) in human lung cancer cell lines, Int. J. Cancer 91 (2001) 468–473.

[3] X. Wu, Y. Chai, R. Yuan, W. Liang, D. Yuan, A novel electrochemiluminescence choline biosensor based on biofunctional AMs-ChO biocomposite, Sens. Actuators B Chem. 204 (2014) 429–436.

[4] J. Liu, Z. Xiong, J. Zhang, C. Peng, X. Shi, Zwitterionic gadolinium (III)-complexed dendrimer-entrapped gold nanoparticles for enhanced CT/MR imaging of lung cancer metastasis, ACS Appl. Mater. Interfaces 11 (2019) 15212–15221.

[5] X. Li, P. Lu, B. Wu, Y. Wang, H. Wang, B. Du, et al., Electrochemiluminescence quenching of luminol by CuS in situ grown on reduced graphene oxide for detection of N-terminal pro-brain natriuretic peptide, Biosens. Bioelectron. 112 (2018) 40–47.

[6] X. Li, D. Wu, H. Ma, H. Wang, Y. Wang, D. Fan, et al., Ultrasensitive amyloid-beta proteins detection based on curcumin conjugated ZnO nanoparticles quenching electrochemiluminescence behavior of luminol immobilized on Au@MoS_2/Bi_2S_3 nanorods, Biosens. Bioelectron. 131 (2019) 136–142.

[7] H. Wang, G. Pu, S. Devaramani, Y. Wang, X. Lu, Bimodal electrochemiluminescence of G-CNQDs in the presence of double co-reactants for ascorbic acid detection, Anal. Chem. 90 (2018) 4871–4877.

[8] Y. Wang, S.Y. Ji, H.Y. Xu, W. Zhao, H.Y. Chen, Bidirectional electrochemiluminescence color switch: an application in detecting multimarkers of prostate cancer, Anal. Chem. 90 (2018) 3570–3575.

[9] J. Xue, L. Yang, Y. Jia, H. Wang, N. Zhang, X. Ren, et al., Electrochemiluminescence double quenching system based on novel emitter GdPO4:Eu with low-excited positive potential for ultrasensitive procalcitonin detection, ACS Sens. 4 (2019) 2825–2831.

[10] M.G. Trachioti, J. Hrbac, M.I. Prodromidis, Determination of Cd and Zn with "green" screen-printed electrodes modified with instantly prepared sparked tin nanoparticles, Sens. Actuators B Chem. 260 (2018) 1076–1083.

[11] S. Liu, J. Zhang, W. Tu, J. Bao, Z. Dai, Using ruthenium polypyridyl functionalized ZnO mesocrystals and gold nanoparticle dotted graphene composite for biological recognition and electrochemiluminescence biosensing, Nanoscale 6 (2014) 2419–2425.

[12] Y.M. Lei, R.X. Wen, J. Zhou, Y.Q. Chai, R. Yuan, Y. Zhuo, Silver ions as novel coreaction accelerator for remarkably enhanced electrochemiluminescence in a PTCA-$S_2O_8^{2-}$ system and its application in an ultrasensitive assay for mercury ions, Anal. Chem. 90 (2018) 6851–6858.

[13] J. Xue, L. Yang, Y. Jia, Y. Zhang, D. Wu, H. Ma, et al., Dual-quenching electrochemiluminescence resonance energy transfer system from Ru-In_2S_3 to alpha-MoO_3-Au based on protect of protein bioactivity for procalcitonin detection, Biosens. Bioelectron. 142 (2019) 111524.

[14] Y. Jia, L. Yang, J. Xue, X. Ren, N. Zhang, D. Fan, et al., Highly-branched Cu_2O as well-ordered co-reaction accelerator for amplifying electrochemiluminescence response of gold nanoclusters and procalcitonin analysis based on protein bioactivity maintenance, Biosens. Bioelectron. 144 (2019) 111676.

[15] W. Huang, G.B. Hu, L.Y. Yao, Y. Yang, W.B. Liang, R. Yuan, et al., Matrix coordination-induced electrochemiluminescence enhancement of tetraphenylethylene-based hafnium metal-organic framework: an electrochemiluminescence chromophore for ultrasensitive electrochemiluminescence sensor construction, Anal. Chem. 92 (2020) 3380–3387.

[16] J.L. Liu, Z.L. Tang, J.Q. Zhang, Y.Q. Chai, Y. Zhuo, R. Yuan, 9 Morphology-controlled, 10-diphenylanthracene nanoblocks as electrochemiluminescence emitters for microRNA detection with one-step DNA walker amplification, Anal. Chem. 90 (2018) 5298–5305.

[17] C.J. Kassl, F. Christopher Pigge, Anion detection by aggregation-induced enhanced emission (AIEE) of urea-functionalized tetraphenylethylenes, Tetrahedron Lett. 55 (2014) 4810–4813.

[18] J.H. Luo, D. Cheng, P.X. Li, Y. Yao, S.H. Chen, R. Yuan, et al., An electrochemiluminescent sensor based on functionalized conjugated polymer dots for the ultrasensitive detection of Cu^{2+}, Chem. Commun. 54 (2018) 2777–2780.

[19] K. Keshav, M.K. Kumawat, R. Srivastava, M. Ravikanth, Benzothiazoles-substituted tetraphenylethylenes: synthesis, structure, aggregation-induced emission and biological studies, Mater. Chem. Front. 1 (2017) 1207–1216.

[20] J.X. Wang, Q. Chen, N. Bian, F. Yang, J. Sun, A.-D. Qi, et al., Sugar-bearing tetraphenylethylene: novel fluorescent probe for studies of carbohydrate–protein interaction based on aggregation-induced emission, Org. Biomol. Chem. 9 (2011) 2219–2226.

[21] J.L. Liu, Y. Zhuo, Y.Q. Chai, R. Yuan, BSA stabilized tetraphenylethylene nanocrystals as aggregation-induced enhanced electrochemiluminescence emitters for ultrasensitive microRNA assay, Chem. Commun. 55 (2019) 9959–9962.

[22] Y. Jia, L. Yang, J. Xue, N. Zhang, D. Fan, H. Ma, et al., Bioactivity-protected electrochemiluminescence biosensor using gold nanoclusters as the low-potential luminophor and Cu_2S snowflake as co-reaction accelerator for procalcitonin analysis, ACS Sens. 4 (2019) 1909–1916.

[23] H. Begam, B. Kundu, A. Chanda, S.K. Nandi, MG63 osteoblast cell response on Zn doped hydroxyapatite (HAp) with various surface features, Ceram. Int. 43 (2017) 3752–3760.

[24] K. Hasna, S.S. Kumar, M. Komath, M.R. Varma, M.K. Jayaraj, K.R. Kumar, Synthesis of chemically pure, luminescent Eu^{3+} doped HAp nanoparticles: a promising fluorescent probe for in vivo imaging applications, Phys. Chem. Chem. Phys. 15 (2013) 8106–8111.

[25] B. Singh, A. Tandon, A.K. Pandey, P. Singh, Enhanced dielectric constant and structural transformation in Fe-doped hydroxyapatite synthesized by wet chemical method, J. Mater. Sci. 53 (2018) 8807–8816.

[26] D. Karthickraja, S. Karthi, G.A. Kumar, D.K. Sardar, G.C. Dannangoda, K.S. Martirosyan, et al., Fabrication of core–shell $CoFe_2O_4$@HAp nanoparticles: a novel magnetic platform for biomedical applications, New J. Chem. 43 (2019) 13584–13593.

[27] H. Zhang, J. Zhou, G.-G. Shan, G.-F. Li, C.-Y. Sun, D.-X. Cui, et al., A tetraphenylethylene-based covalent organic polymer for highly selective and sensitive detection of Fe^{3+} and as a white light emitting diode, Chem. Comm. 55 (2019) 9955–9962.

[28] X. Zhang, P.Z. Chi, D.H. Li, D.B. Xu, D.X. Li, W. Zhou, et al., Piezofluorochromism of an aggregation-induced emission compound derived from tetraphenylethylene, Chem. Asian J. 6 (2011) 808–811.

[29] L. Yang, J. Xue, Y. Jia, Y. Zhang, D. Wu, H. Ma, et al., Construction of well-ordered electrochemiluminescence sensing interface using peptide-based specific antibody immobilizer and N-(aminobutyl)-N-(ethylisoluminol) functionalized ferritin as signal indicator for procalcitonin analysis, Biosens. Bioelectron. 142 (2019) 111562.

[30] C. Guo, X. Liu, L. Gao, X. Kuang, X. Ren, X. Ma, et al., Fe-doped Ni_2P nanosheets with porous structure for electroreduction of nitrogen to ammonia under ambient conditions, Appl. Catal. B: Environ. 263 (2020), https://doi.org/10.1016/j.apcatb.2019.118296.

[31] C.Y. Jeong, B.J. Young, K.S. Hoon, K. Jongsik, Fe_3S_4/Fe7S8-promoted degradation of phenol via heterogeneous, catalytic H_2O_2 scission mediated by S-modified surface Fe^{2+} species, Appl. Catal. B Environ. 233 (2018) 272–280.

[32] E. Ferreira, N.T.C. Oliveira, S.R. Biaggio, P.A.P. Nascente, N. Bocchi, XPS characterization of anodic oxides grown on biocompatible Ti–50Zr alloy in different acid electrolytes, Surf. Interface Anal. 38 (2006) 417–421.

[33] J. Xue, L. Yang, H. Wang, T. Yan, D. Fan, R. Feng, et al., Quench-type electrochemiluminescence immunosensor for detection of amyloid beta-protein based on resonance energy transfer from luminol@SnS_2-Pd to Cu doped WO_3 nanoparticles, Biosens. Bioelectron. 133 (2019) 192–198.

[34] C. Cheng, Y. Huang, X. Tian, B. Zheng, Y. Li, H. Yuan, et al., Electrogenerated chemiluminescence behavior of graphite-like carbon nitride and its application in selective sensing Cu^{2+}, Anal. Chem. 84 (2012) 4754–4759.

Jingwei Xue studies in school of chemistry and chemical engineering, University of Jinan as postgraduate student.

Lei Yang studies in school of chemistry and chemical engineering, University of Jinan as doctoral student.

Yu Du works and studies in School of Chemistry and Chemical Engineering, University of Jinan as a teacher. Her main research interests are the determination of electrochemiluminescence immunosensor.

Yong Ren works and studies in Department of Mathematical Sciences, Zibo Normal College, as a teacher.

Xiang Ren received his B.S. degree in Chemistry of Materials from University of Jinan in 2012, M.S. degree in Chemical Engineering and Technology from University of Jinan in 2015 and Ph.D. degree from University of Jinan/University of Electronic Science and Technology of China in 2019. Now, he is an associate professor in University of Jinan. His main research interests are energy catalysis, nanomaterials controlled-synthesis, and electrochemical biosensors.

Hongmin Ma received both his B.S. and M.S. degree in Applied Chemistry from University of Jinan in 2005 and 2008 respectively. And he has received his Ph.D. degree in Colloid and Interface Chemistry at Shandong University, investigating self-assembly at all scales at surfaces in 2011. Now, he is a professor at University of Jinan, interested in the assembly of nano-composites and the construction of ordered porous films as well as their analytical applications.

Dan Wu a professor and received the D.S. degree from Shandong University in 2005. She dedicates to the surfactant and biological macromolecules interaction. And now she also studies the role of surfactant in electrochemical immunosensor.

Huangxian Ju received his BS, MS and PhD degrees from Nanjing University during 1982–1992. He was a postdoc in Montreal University (Canada) in 1996–1997 and a guest professor in three universities of Germany and Ireland in 1999 – 2000. He became an associate and full professor of Nanjing University in 1993 and 1999. He is currently the director of State Key Laboratory of Analytical Chemistry for Life Science. His research interests focus on analytical biochemistry, biosensing and molecular diagnosis. He has published 635 papers in different journals with h-index of 85 (Google Scholar h-index 95 with about 31634 citations).

Yueyuan Li is a current Ph. D. student, studies in School of Chemistry and Chemical Engineering, University of Jinan. She is working on constructing immunosensor.

Qin Wei, a professor and DSc, has devoted herself to analytical teaching and scientific research. Her main research interests are the determination of protein and nucleic acid by photometry and the electrochemical immunosensor preparation. She has published over two hundred articles on analysis, immunosensor and applied successfully for many research projects, such as *Biomaterials, Advanced Functional Materials., Biosensors & Bioelectronics, Sensors and Actuators B: Chemical, ACS Applied Materials & Interfaces, and Talanta*.